Wave propagation in randomly parameterized 2D lattices via machine learning

Tanmoy Chatterjee[a,*], Danilo Karličić[b], Sondipon Adhikari[a], Michael I. Friswell[a]

[a] *College of Engineering, Swansea University, United Kingdom*
[b] *Mathematical institute of the Serbian Academy of Sciences and Arts, Kneza Mihaila 36, Belgrade, Serbia*

Abstract

Periodic structures attenuate wave propagation in a specified frequency range, such that a desired bandgap behaviour can be obtained. Most periodic structures are produced by additive manufacturing. However, it is recently found that the variability in the manufacturing processes can lead to a significant deviation from the desired behaviour. This paper investigates the elastic wave propagation of stochastic hexagonal periodic lattice structures considering micro-structural variability. Thus, the effect of uncertainties in the material and geometrical parameters of the unit cell is quantified on the wave propagation in hexagonal lattices. Based on Bloch's theorem and the finite element method, the band structures are determined as a function of the frequency and wave vector at the unit cell level and later scaled-up via full-scale simulations of finite metamaterials with a prescribed number of cells. State of the practice machine learning techniques, namely the Gaussian process, multi-layer perceptron, radial basis neural network and support vector machine, are employed as grey-box meta-models to capture the stochastic wave propagation response. The results demonstrate good accuracy by validation with Monte Carlo simulations. The study illustrates that considering the effect of uncertainties on the wave propagation behaviour of hexagonal periodic lattices is critical for their practical applicability and desirable performance. Based on the results, the manufacturing tolerances of the hexagonal lattices can be obtained to attain a bandgap within a certain frequency band.

Keywords: Manufacturing variability; Hexagonal lattice; Wave propagation; Machine learning; Bloch theorem

1. Introduction

Lattice materials are periodic structures formed by tessellating a chosen unit cell, which can be either rigidly connected or joined through pins. These materials with different topologies have been the subject of considerable attention, as they are simplified models of a number of structural systems found in various engineering fields [1, 2]. A few examples of lattice-like materials and systems include, but are not limited to, honeycomb structures, periodic trusses, acoustic metamaterials and periodic lattice structures with local resonators. The mechanical properties of lattices derive great leverage from the spatial periodicity of their structural building blocks [3]. This has led to superior properties in periodic structures compared to conventional materials found in nature [4]. Additionally, the fast growing additive manufacturing technology

*Corresponding author
Email address: tanmoy.chatterjee@swansea.ac.uk (Tanmoy Chatterjee)

has enabled ways of easy and rapid realization of the complex geometry, allowing novel and innovative means to design and manufacture metamaterials.

These mechanical structures have intervals of frequency for which there is no propagation of elastic waves, referred to as 'stop-bands' or 'bandgaps' [5]. Tuning the wave dispersion characteristics of metamaterials, what can be called as 'bandgap engineering' often involve, opening, closing, enlarging or shifting bandgaps in specific target frequency regions. In this regard, wave propagation of mechanical metamaterials has received immense popularity due to their practical applications as filters and insulators in vibration isolation and energy harvesting. Therefore, as expected, the literature is abundant with the above related studies, however, mostly based on the underlying assumption that the set of parameters required to determine the wave dispersion behaviour is precisely known.

In the above context, few recently conducted studies on deterministic wave propagation analysis of periodic lattices are briefly discussed next. The effect of pre-load on the wave propagation of hexagonal lattices was investigated in [6]. Vibroacoustic analysis was carried out for auxetic gradient composite hexagonal honeycombs in [7]. The mechanism of directional wave propagation in auxetic chiral lattices was studied in [8]. In [9], the wave propagation in a pre-stressed and elastically embedded hexagonal lattice structure with attached point masses was investigated. Wave propagation in composite X-lattice structures comprising corrugated carbon-fiber-reinforced plastic ribs was studied in one dimension [10] and two dimensions [11]. Wave propagation of a lightweight adaptive hybrid laminate comprising carbon-fiber-reinforced polymer and a periodic array of piezoelectric shunting patches [12]. The inertial amplification mechanisms were applied to the composite sandwich beam with lattice truss cores to obtain multiple and wider bandgaps [13]. Multiscale analysis of elastic properties and band-gaps of microtruss lattice materials was carried out in [14]. Dispersion behaviour of periodic structures was studied using higher order beam element dynamics for the accurate representation of higher wave propagation modes [15] and nonlinear effects such as the wave amplitude-dependent dispersion phenomena [16]. Nonlinear wave propagation of periodic designs was investigated using second order gradient-enriched constitutive models [17] and non-slender structural design [18]. Prestrain induced bandgap tuning in tensegrity lattices was studied in [19–21]. Wave control by smart micro-structural shape modification [22], and thermally tunable composite metastructures [23] are couple of examples of active tuning of wave dispersion characteristics in periodic structures.

The requirement of an ideal periodic configuration creates several challenges related to the precision of the fabrication of lattice structures, which intuitively suffer from anomalies such as machining tolerances, and surface roughness [24]. Consequently, a series of perfectly identical unit cells cannot be practically realized in the presence of inevitable manufacturing uncertainties, which eventually leads to undesirable performance variations. In fact, most nano, micro and macrostructures fabricated using e-beam lithography, etching and milling processes, respectively are vulnerable to manufacturing uncertainties. Even the optimized structures may experience inferior performance or in an extreme scenario, lose their functionality due to the wear of machining tools, under or over-etching, or malcalibrated e-beam equipment [25]. However, in some cases, it has been observed that randomness may enhance the performance of meta-materials [26]. Therefore, the industrial application of periodic structures is quite rare, and one potential reason is the variability associated with their micro-structural properties [27]. One of the few related works considering the robust optimal design of seismic metamaterials is [28]. The influence of point defects in a phononic crystal Timoshenko beam [29] and periodic crystal thin plates [30] were investigated. It was shown that the defect modes in the first bandgap are primarily dependent on the size of the point defects and the filling fraction of the system. The wave finite

element method was utilized to analyze locally perturbed one-dimensional periodic structures in [31]. The effect of randomly fractured unit cell walls was analyzed on the wave propagation characteristics of periodic lattices. The correlation of the velocity of surface waves with the amount of damage within lattices was also quantified [32, 33].

Uncertainty quantification (UQ) has been investigated using two broad classes of methods, namely sampling and non-sampling based techniques. Monte Carlo simulation (MCS) is a popular sampling-based approach in which a large number of realizations of stochastic parameters are required to obtain the response variation. Although straightforward to use, MCS is computationally expensive. In contrast, meta-modelling is a non-sampling based technique where the functional dependence of an implicit system response is captured by an algebraic expression. The book by Dey et. al. [34] gives a comprehensive overview of different meta-modelling approaches for the dynamics of structures with uncertainties. The influence of uncertainties in geometric parameters, such as plate thickness, resonator radius and resonator length, on the centre position and the bandgap width was studied in [27] by a spectral method based on generalized polynomial chaos (gPC). Uncertainties were evaluated at the unit-cell dispersion level and then via full-scale simulations of finite meta-materials with a prescribed number of cells and a scheme which ensures the desired bandgap [35]. Three different configurations were analyzed using gPC, namely (i) periodic structures with periodic variations, representative of conventional phononic crystals, (ii) a lattice with a periodic elastic foundation, and (iii) a locally resonant meta-material. Approximation of close modes in periodic structures featuring mode degeneration under uncertainty was presented in [36]. A stochastic finite-element model of acoustic metamaterials with random parameters was given in [37] using a first-order Taylor series expansion and perturbation technique. An optimal disorder degree was shown in [38] below which the attenuation bandwidth widens and for high disorder levels, the bandgap mistuning annihilates the overall attenuation. Experiments have estimated the manufacturing tolerances of metamaterial samples produced by a selective laser sintering process [39] to simulate the manufacturing uncertainty in mass-produced industrial applications. The resulting spatial variability was used to construct a random field model for the metamaterial. It was found that even small levels of variability, given by less than 1% for the mass and less than 3% for the elastic modulus, has a significant effect on the overall vibration attenuation performance.

In this work, stochastic wave propagation of hexagonal lattice structures is performed to quantify the effect of input micro-structural parametric uncertainty on the dynamic behaviour. For doing so, the simulations are performed at the unit-cell dispersion level and are later corroborated via full-scale simulations of finite metamaterials with a prescribed number of cells. The proposed approach develops and tunes the optimal configuration of state of the practice machine learning (ML) models, which can emulate the original stochastic system inexpensively, and thus accurately determine the variation in the wave responses. To the best of the authors' knowledge, this is one of the first applications of ML in meta-modelling for the stochastic wave response of hexagonal lattice structures considering their micro-structural variability. Two recent studies with a similar framework include, application of neural networks in mapping the material tensors of a phononic crystal to its eigenvalues [40] and radial basis function assisted optimal design of tetrachiral microstructure [41]. However, these were implemented in a data-driven context and do not consider any form of model uncertainty.

2. Mathematical preliminaries

2.1. 2D lattice structures

To determine the free in-plane wave propagation through a typical two dimensional lattice structure with randomly distributed parameters, we consider the hexagonal type lattice structure shown in Fig. 1. The presented hexagonal structure is composed of a periodically distributed unit cell, which consists of three rigidly connected elastic thick beams, as shown in Fig. 1(a) and (b). In this analysis, the Timoshenko beam model is adopted. The mechanical model of the unit cell of the hexagonal periodic structure with the characteristic dimensions, is given in Fig. 1(b). The internal angle of the unit cell is defined as θ, and by changing this angle the hexagonal lattice structure can be transformed into a re-entrant honeycomb when θ is negative. The main geometrical characteristics of the unit cell is the wall slenderness ratio defined as $\beta = d/L$. The wall slenderness ratio controls the Bloch wave propagation and design of the wave filters for specific frequency ranges. A regular hexagonal lattice has the internal angle, $\theta = 30°$. Lattice structures are obtained by periodically distributing the chosen unit cell, where the connection nodes are known as lattice points in direct lattice space. For two-dimensional structures there are two basis vectors $(\mathbf{e}_1, \mathbf{e}_2)$, which define the primitive unit cell and connect with other unit cells. Therefore, the problem of wave propagation in periodic lattice structures can be reduced to a typical unit cell by introducing periodic boundary conditions according to Bloch's theorem. The local coordinates of the single beam model is adopted such that the x coordinate is taken along the length of the beam and the z coordinate is in the thickness direction of the beam.

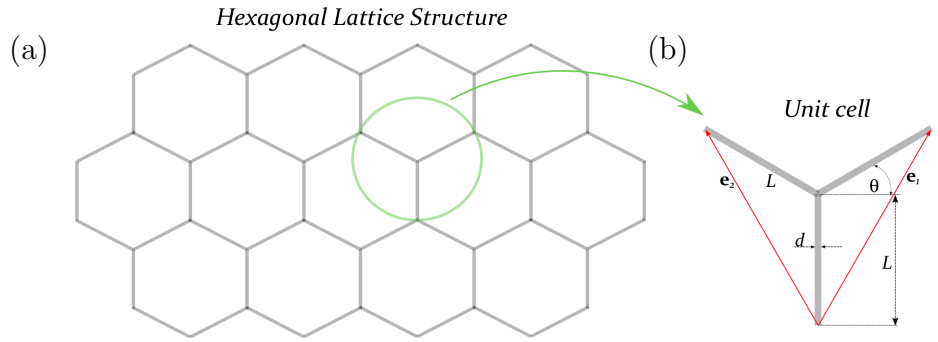

Figure 1: Mechanical model of a hexagonal lattice composed of Timoshenko beams: a) the two-dimensional hexagonal lattice, b) the unit cell.

The unit cell of the hexagonal lattice structure with positive internal angle, θ, has base vectors $(\mathbf{e}_1, \mathbf{e}_2)$ defined in the local rectangular coordinate system with unit vectors $(\mathbf{i}_1, \mathbf{i}_2)$, given by

$$\begin{aligned} \mathbf{e}_1 &= [L\cos\theta, L(1+\sin\theta)]^T \\ \mathbf{e}_2 &= [-L\cos\theta, L(1+\sin\theta)]^T \end{aligned} \tag{1}$$

The base vectors $(\mathbf{e}_1, \mathbf{e}_2)$ define the direct lattice space and the reciprocal lattice space may be defined from

$$\mathbf{e}_i^T \mathbf{e}_j^* = \delta_{ij}, \tag{2}$$

where $\mathbf{e}_j^*$ represents the basis vectors of the reciprocal lattice, and δ_{ij} is the Kronecker delta. The

reciprocal lattice vectors for the hexagonal lattices structure and chosen unit cell, are defined as

$$\mathbf{e}_1^* = \left[\frac{1}{2L\cos\theta}, \frac{1}{2L(1+\sin\theta)}\right]^T \tag{3}$$
$$\mathbf{e}_2^* = \left[-\frac{1}{2L\cos\theta}, \frac{1}{2L(1+\sin\theta)}\right]^T$$

2.2. Bloch's theorem

Bloch's theorem is a generalization of Floquet theory which has applications in quantum mechanics to solve Schrödinger's equation [42], and has been extended to analyze waves in macroscopic periodic elastic structures [43, 44]. The elastic wave propagates through the infinite periodic lattice structure formed by tessellating the unit cell along the basis vectors $(\mathbf{e}_1, \mathbf{e}_2)$ connected at the lattice points. By considering Bloch's theorem, the analysis of the wave propagation in the infinite structure can be reduced to the chosen unit cell. The position of the primitive unit cell is determined by the vector, $\mathbf{s} = \mathbf{r} + n\mathbf{e}_1 + m\mathbf{e}_2$, placed in the plane of the lattice structure [45]. The integer pair (n, m) determines position of the unit cell along the basis vectors $(\mathbf{e}_1, \mathbf{e}_2)$. The vector $\mathbf{r}$ is the position of any point inside the reference primitive unit cell determined by $(n, m) = (0, 0)$. The displacement vector corresponding to a wave at an arbitrary point inside the reference unit cell is given by $\mathbf{w}(\mathbf{r}) = \mathbf{w}_r e^{i\omega t - \mathbf{k}\cdot\mathbf{r}}$, where the frequency of the wave is ω (in rad/s), $\mathbf{w}_r$ is related to the wave amplitude, and $\mathbf{k}$ is the wave vector of the plane wave.

Consider the unit cell determined by the integers (n, m), where n is the number of unit cells along the direction $\mathbf{e}_1$ and m is the number of unit cells along the direction $\mathbf{e}_2$. The displacement vector of point $\mathbf{s}$ inside the chosen unit cell is defined as

$$\mathbf{w}(\mathbf{s}) = \mathbf{w}(\mathbf{r})e^{\mathbf{k}\cdot(\mathbf{s}-\mathbf{r})} = \mathbf{w}(\mathbf{r})e^{\mathbf{k}\cdot(n\mathbf{e}_1+m\mathbf{e}_2)}, \tag{4}$$

where $\mathbf{k}\cdot\mathbf{e}_i = k_i$ and $i = 1, 2$.

The elastic wave propagation properties of the periodic system can be described by only one unit cell with corresponding boundary conditions where Bloch waves exist. Consequently, the application of Bloch's theorem can save significant computational cost. This can be viewed as a type of model reduction for periodic structures. The wave numbers $k_i, (i = 1, 2)$ given in Eq. (4), are complex numbers of the form $k_i = \phi_i + \mathrm{i}\epsilon_i, (i = 1, 2)$, where the real part ϕ_i is related to the amplitude attenuation as a wave propagates from one cell to the next. The imaginary part ϵ_i is related to the change in phase across each cell and is known as the phase constant. For Bloch waves propagating through the unit cell, it is assumed that the waves propagate without attenuation, and hence the real part ϕ_i is set to 0. The relation between ω and (k_1, k_2) is known as the dispersion surface, where each surface is related to different modes of elastic wave propagation through the periodic structure.

2.3. Solution approach

The periodic structure considered consists of a repetitive unit cell modelled as Timoshenko beams. The complete finite element (FE) formulation of the unit cell can be found in [9]. The solution process using Bloch's theorem is reduced to the determination of an eigenvalue problem. Introducing the harmonic solution $\mathbf{q}(x, t) = \mathbf{q}(x)e^{i\omega t}$ into the FE model of the unit cell yields,

$$\left[\mathbf{K} - \omega^2\mathbf{M}\right]\mathbf{q} = \mathbf{f} \tag{5}$$

where $\mathbf{f}$ is the force vector resulting from the interaction between the cells, and ω is the frequency of free wave propagation. The generalized coordinate vector $\mathbf{q}$ is a set of nodal displacements

that may be written in the form

$$\mathbf{q} = \begin{Bmatrix} \mathbf{q}_0 \\ \mathbf{q}_1 \\ \mathbf{q}_2 \\ \mathbf{q}_i \end{Bmatrix} \tag{6}$$

where $\mathbf{q}_0$, $\mathbf{q}_1$ and $\mathbf{q}_2$ represent the nodal displacements at the end nodes of the unit cell. The nodal displacements $\mathbf{q}_i$ correspond to the degrees of freedom of the internal nodes of the unit cell. Considering free wave propagation leads to the absence of external forces on the internal nodes and significantly reduces the computation requirements. Based on Bloch's theorem, periodic boundary conditions are applied to the unit cell, and in particular applied to the displacements of the end nodes as

$$\mathbf{q}_1 = e^{k_1}\mathbf{q}_0, \qquad \mathbf{q}_2 = e^{k_2}\mathbf{q}_0. \tag{7}$$

Eq. (7) yields a transformation matrix that can be applied to the global vector of nodal displacements as

$$\mathbf{q} = \mathbf{T}_b\mathbf{q}_r, \tag{8}$$

where the global vector of nodal displacements is reduced to $\mathbf{q}_r = \begin{Bmatrix} \mathbf{q}_0 \\ \mathbf{q}_i \end{Bmatrix}$, and the matrix $\mathbf{T}_b$ is defined as

$$\mathbf{T}_b = \begin{bmatrix} \mathbf{I} & \mathbf{0} \\ \mathbf{I}e^{k_1} & \mathbf{0} \\ \mathbf{I}e^{k_2} & \mathbf{0} \\ \mathbf{0} & \mathbf{I} \end{bmatrix}. \tag{9}$$

Substituting Eq. (8) into Eq. (5), and pre-multiplying the resulting expression with the Hermitian transpose (complex transpose conjugate) matrix $\mathbf{T}_b^H$, yields

$$\left[\mathbf{K}_r(k_1,k_2) - \omega^2\mathbf{M}_r(k_1,k_2)\right]\mathbf{q}_r = \mathbf{T}_b^H\mathbf{f} = \mathbf{0}, \tag{10}$$

where

$$\begin{aligned} \mathbf{M}_r(k_1,k_2) &= \mathbf{T}_b^H\mathbf{M}\mathbf{T}_b \\ \mathbf{K}_r(k_1,k_2) &= \mathbf{T}_b^H\mathbf{K}\mathbf{T}_b \end{aligned} \tag{11}$$

and $\mathbf{T}_b^H\mathbf{f} = \mathbf{0}$ due to periodicity.

In order to determine the dispersion curves and corresponding frequency band structure diagrams, the eigenvalue problem given in Eq. (10) has to be solved for various values of the wave numbers $k_i, (i = 1, 2)$, restricted to the First Brillouin Zone (FBZ), and the solutions will be presented as $\omega = \omega(k_1, k_2)$. The computational effort can be substantially reduced by exploiting the symmetry of the FBZ as well as the unit cell as stated in [43]. From the physical point of view, the geometrical shape of the FBZ is directly dependent on the internal lattice angle θ, and can form a uniquely defined primitive cell in reciprocal space denoted by vectors $(\mathbf{e}_1^*, \mathbf{e}_2^*)$. For more detail about the symmetry and their application in the FBZ, interested readers are referred to [46, 47]. This reduced part of the FBZ is also known as the irreducible Brillouin zone (IRBZ). For the hexagonal structure, the IRBZ and its contours are shown as the shaded region defined by $O-A-B-C-O$ in Fig. 2. For our subsequent analysis, the formation of the band structures is based on the restricted zone of the IRBZ in the reciprocal lattice frame with coordinates of the boundary points $(O - A - B - C - O)$ as given in [47].

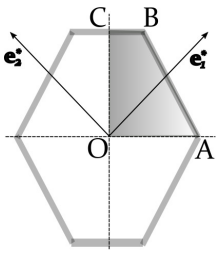

Figure 2: The first Brioullin zone for the regular hexagonal unit cell.

3. Meta-modelling via machine learning

When uncertainties in the system are considered, the deterministic eigenvalue problem defined in Eq. (10) becomes a random eigenvalue problem (see for example [48, 49]). A straightforward approach to propagate the input uncertainties on the wave response of the periodic system involves a large number of repeated simulations on the actual system. Specifically, one has to solve a random eigenvalue problem for each value of the wave vector. Therefore, solving an eigenvalue problem for every value of the wave vector corresponding to each random realizations of the input uncertainty can prove to be computationally expensive. To avoid performing the eigenvalue analysis on the actual system and reduce the computational cost, ML techniques have been employed here as physics-based meta-models to capture the variation in the wave response. It will also be an interesting exercise to tune the network parameters and obtain their optimal configuration to access their approximation accuracy, because the wave response of lattice structures is very sensitive to input uncertainties. Another advantage is that the trained ML techniques can be used as emulators of the wave behaviour in the lattice structures and can be used on any unseen datasets or augment additional data without having to train the networks from scratch (transfer learning). A brief description of the ML techniques used in this work is provided next.

3.1. Gaussian process (GP)

The Gaussian process (GP) is a stochastic process which stipulates probability distributions over functions. Originally GP was developed as a spatial interpolation technique in the field of geostatistics [50] and later applied in the dynamics of structures [51, 52] and probabilistic finite element models [53]. GP is also known as Kriging in several disciplines [54, 55]. Considering an independent variable $\mathbf{x} \in \mathbb{R}^d$ and function $g(\mathbf{x})$ such that $g : \mathbb{R}^d \to \mathbb{R}$, a GP over $g(\mathbf{x})$ with mean $\mu(\mathbf{x})$ and covariance function $\kappa(\mathbf{x}, \mathbf{x}'; \Theta)$ can be defined as

$$\begin{aligned} g(\mathbf{x}) &\sim GP(\mu(\mathbf{x}), \kappa(\mathbf{x}, \mathbf{x}'; \Theta)), \\ \mu(\mathbf{x}) &= \mathbb{E}[g(\mathbf{x})] \\ \kappa(\mathbf{x}, \mathbf{x}'; \Theta) &= \mathbb{E}[(g(\mathbf{x}) - \mu(\mathbf{x}))(g(\mathbf{x}') - \mu(\mathbf{x}'))] \end{aligned} \tag{12}$$

where Θ denotes the hyperparameters of the covariance function κ. The choice of the covariance function κ allows to incorporate any prior knowledge about $g(\mathbf{x})$ (for instance, periodicity, linearity, smoothness) and can cope with the approximation of arbitrary complex functions. The covariance function brings in interdependencies between the function value corresponding to different inputs. For instance, the following squared exponential (Gaussian) covariance function is used in this study.

$$\kappa(\mathbf{x}, \mathbf{x}') = \sigma_g^2 \exp\left[-\sum_{i=1}^{d} \frac{(x(i) - x'(i))^2}{2r_i^2} \right] \tag{13}$$

where $\{\sigma_g, r_1, \ldots, r_d\} = \Theta$ are the hyperparameters of the covariance function.

One perspective of viewing GP is the function-space mapping describing the input-output relationship [56]. As opposed to conventional modelling techniques which employ fitting a parameterized mathematical form to map the input-output functional space, a GP does not assume any explicit form, and instead holds a prior belief (in the form of the mean and covariance function) onto the space of model (response) functions. Thus, GPs can be classified as a 'non-parametric' model as the number of parameters in the model is governed by the number of available data points.

The most general form of GP, called Universal Kriging, is used in this study [57]. This can be represented by second-order polynomial trend functions and can be expressed as

$$\mathbf{y}(\mathbf{x}) = \sum_{j=1}^{p} \beta_j \mathbf{f}_j(\mathbf{x}) + \mathbf{z}(\mathbf{x}) \tag{14}$$

where $\boldsymbol{\beta} = \{\beta_j, j = 1, \ldots, p\}$ is the vector of unknown coefficients and $\mathbf{F} = \{\mathbf{f}_j, j = 1, \ldots, p\}$ is the matrix of polynomial basis functions. $\mathbf{z}(\mathbf{x})$ is the GP with zero mean and autovariance $\text{cov}[\mathbf{z}(\mathbf{x}), \mathbf{z}(\mathbf{x}')] = \sigma^2 \mathbf{R}(\mathbf{x}, \mathbf{x}')$, where σ^2 is the process variance and $\mathbf{R}(\mathbf{x}, \mathbf{x}')$ is the autocorrelation function.

The parameters $\boldsymbol{\beta}$ and σ^2 can be estimated by the maximum likelihood estimate (MLE) defined by the following optimization problem under the assumption that the noise $\mathbf{z} = \mathbf{y} - \mathbf{F}\boldsymbol{\beta}$ is a correlated Gaussian vector

$$(\hat{\boldsymbol{\beta}}, \hat{\sigma^2}) = \arg\max_{\boldsymbol{\beta}, \sigma^2} \mathbf{L}(\boldsymbol{\beta}, \sigma^2 | \mathbf{y}) = \frac{1}{((2\pi\sigma^2)^n \det\mathbf{R})^2} \exp\left[-\frac{1}{2\sigma^2}(\mathbf{y} - \mathbf{F}\boldsymbol{\beta})^T \mathbf{R}^{-1} (\mathbf{y} - \mathbf{F}\boldsymbol{\beta})\right] \tag{15}$$

Upon solving Eq. (15), the estimates $(\hat{\boldsymbol{\beta}}, \hat{\sigma^2})$ can be obtained as

$$\hat{\boldsymbol{\beta}} = (\mathbf{F}^T \mathbf{R}^{-1} \mathbf{F})^{-1} \mathbf{F}^T \mathbf{R}^{-1} \mathbf{y} \tag{16}$$

$$\hat{\sigma^2} = \frac{1}{n}(\mathbf{y} - \mathbf{F}\boldsymbol{\beta})^T \mathbf{R}^{-1} (\mathbf{y} - \mathbf{F}\boldsymbol{\beta}) \tag{17}$$

where $\mathbf{y}$ represents the model response such that $\mathbf{y} = \{y_1, \ldots, y_n\}^T$.

The prediction response for a test point requires three conditions to be satisfied, which are linearity in terms of the observed data, unbiasedness and minimal variance. The prediction mean and variance by GP can be obtained as

$$\mu_{\hat{Y}}(\mathbf{x}) = \mathbf{F}^T \hat{\boldsymbol{\beta}} + \mathbf{r}^T \mathbf{R}^{-1} (\mathbf{y} - \mathbf{F}\hat{\boldsymbol{\beta}}) \tag{18}$$

$$\sigma^2_{\hat{Y}}(\mathbf{x}) = \hat{\sigma^2}[1 - \mathbf{r}^T \mathbf{R}^{-1} \mathbf{r} + \mathbf{u}^T (\mathbf{F}^T \mathbf{R}^{-1} \mathbf{F})^{-1} \mathbf{u}] \tag{19}$$

where $\mathbf{u} = \mathbf{F}^T \mathbf{R}^{-1} \mathbf{r} - \mathbf{R}$ and $\mathbf{r}$ is the autocorrelation between the unknown point $\mathbf{x}$ and each point of the observed data set.

Some unique features of the above formulation are: (i) The prediction is exact at the training points and the associated variance is zero. (ii) It is asymptotically zero which means that as the size of the observed data set increases, the overall variance of the process decreases. (iii) The prediction at a given point is considered as a realization of a Gaussian random variable. Thus, it is possible to derive confidence bounds on the prediction. The variance information is often used as an error measure of the epistemic uncertainty of the meta-model due to sparsity of data [58]. This feature has led to the development of adaptive error based sampling schemes for improving the accuracy of the meta-model [59].

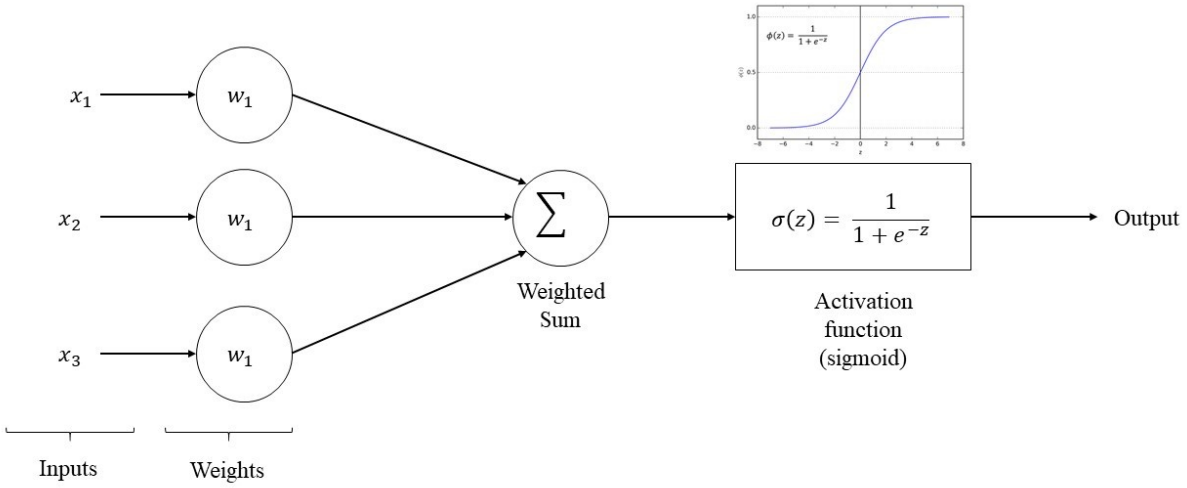

Figure 3: Schematic representation of the basic process in a single neuron.

3.2. Multi-layer perceptron (MLP)

Artificial Neural Networks (ANN) are considered as complex predictive models, due to their ability to handle multi-dimensional data, non-linearity, and adept learning ability and generalisation [60]. The basic framework of a neural network comprises four atomic elements, namely: (i) nodes, (ii) connections/weights, (iii) layers, and (iv) activation function. In the MLP, the neurons represent the building blocks. These neurons, which are simple processing units, each have weights that return weighted signals and an output signal, which is achieved using an activation function. The MLP reduces error by optimisation algorithms or functions, such as backpropagation [61, 62].

In an MLP, the set of nodes are connected together by weighted connections, which can be analogous to the coefficients in a regression equation. These weighted connections represent the connecting interactions. The optimal weights of each connection between a set of layers are calculated during each backward pass of a training dataset, which is also used for weight optimisation using the derivatives obtained from the input and predicted values of the training data. The layers represent the network topology, representing neuron interconnections. Within the network, the transfer function or activation function represents the transfer function or state of each neuron. The basic process in a single neuron is presented in Fig. 3. In the MLP, an external input vector is fed into the model during training. In the case of binary classification problems, during the training, the output is clamped to either 0 or 1, via the sigmoid activation function. A particular variation of neural networks is the feed-forward neural network. This is widely used in modelling many complex tasks, with the generic architecture depicted in Fig. 4. As the figure shows, the elementary model structure comprises three layers, namely the input, hidden, and output layers respectively. In Feed-forward Neural Networks (FFNN), each individual neuron is interconnected to the output of each unit within the next layer.

Consequently, it has been proven that an MLP, trained to minimise a loss or cost function between an input and output target variable using sufficient data, can accurately produce an

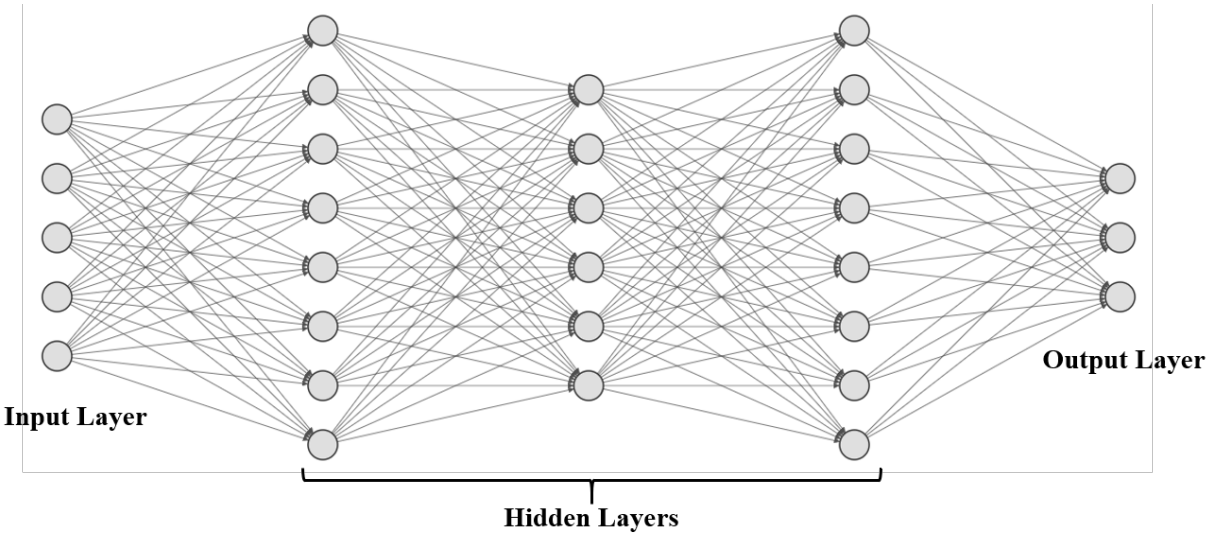

Figure 4: Multi-task deep neural network adopted in this study.

estimate of the posterior probability of the output classes based on the discriminative conditioning of the input vector, which is then applied approach in this study.

3.3. Support vector machine (SVM)

Classical learning algorithms are trained by minimising the error on the training dataset and this process is called empirical risk minimisation (ERM). Many machine learning algorithms learn using ERM, such as neural networks and regression-based algorithms. However, the support vector machine is based on minimising the structural risk minimisation (SRM) principle, a statistically-relevant method. Some studies have proven that this method results in improved generalisation performance, given that the SRM is obtained by reducing the upper bound of the generalisation error [63, 64]. The support vector algorithm was developed by Russian statisticians Vapnik and Lerner [65].

To describe the inner working of the SVM, consider input data $\mathbf{x} = \{x_1, x_2, \ldots, x_n\}$, where n represents the number of samples having two distinct classes (i.e. True and False). Assume each class associated to label $y_i = 1$ for true and $y_i = 0$ for the negative class. For linear input data, we define a hyperplane $f(\mathbf{x}) = 0$ that separates the given data. We define a linear function f of the form:

$$f(\mathbf{x}) = \mathbf{w}^T\mathbf{x} + b = \sum_{j=1}^{m} w_j x_j + b = 0, \tag{20}$$

where $\mathbf{w} \in \mathbb{R}^{n\times 1}$, and b is a scalar. Together, the vector $\mathbf{w}$ and b can be used to define the position of the hyperplane. The output of the model uses $f(\mathbf{x})$ to create a hyperplane that classifies the input data to either class (i.e. True or False). It is important to note that, for an SVM, the satisfying conditions for the hyperplane can be presented as

$$y_i f(x_i) = y_i(\mathbf{w}^T x_i + b) \geq 1, i = \{1, 2, \ldots, n\} \tag{21}$$

For non-linear classification tasks, the kernel-based SVM can be adopted. In this case, the data to be classified is mapped to a high-dimensional feature space where linear separation using a hyper-plane is possible. Consider a non-linear vector, $\mathbf{\Phi}(\mathbf{x}) = (\boldsymbol{\phi}_1(\mathbf{x}), \ldots, \boldsymbol{\phi}_l(\mathbf{x}))$, which can be used to map the m-dimensional input vector $\mathbf{x}$ to an l-dimensional feature space. The linear

decision function, therefore, used to make this transformation can be given as

$$f(\mathbf{x}) = \text{sign}\left(\sum_{i,j=1}^{n} \alpha_i y_i(\mathbf{\Phi}(x_j))\right) + b \tag{22}$$

Although using SVM for non-linear classification by working in the high-dimensional feature space results in benefits, for instance, in modelling complex problems, there are drawbacks, brought about by excessive computational requirements and overfitting.

4. Results and discussion

4.1. Analysis at the unit cell level

Wave propagation in hexagonal lattice structures has been studied considering micro-structural variability. For doing so, the material and geometric parameters of the unit cell of the lattice model are considered as random. As the unit cell is repeated infinitely, the analysis with uncertain inputs in this unit cell can be interpreted as an analysis of different specimens wherein one specimen of all periodic structures are identical [27]. This analysis is intended towards identifying the influence of tolerances which results from repeated additive manufacturing processes. However, the changes due to the uncertainty have to be nominally identical for each unit cell within the periodic structure. Another important question is the consideration of uncertainties within one specimen. As the unit cell is assumed to be repeated infinitely, this may not be a suitable model to investigate this question. Investigation of dispersion curves and their topology, leading to the detection of the pass and stop bands by using the Bloch wave analysis for a chosen unit cell configuration, is based on a solution of the corresponding eigenvalue problem. This insight into the band structure of the lattice system allows us to passively control elastic wave propagation.

In the numerical simulations, the material and geometrical parameters are the same as adopted in [45]. The cross-sectional area $A = bh$, the second moment of inertia $I = \frac{bh^3}{12}$ and the wall's slenderness ratio $\beta = d/L = 1/15$. Length of all the beams is $L = 0.125$ m, $\rho = 25 \cdot 10^3$ kg/m^3 is the mass density, $E = 210 \cdot 10^9$ Pa denotes the elastic modulus, $\nu = 0.25$ is the Poisson's ratio. For clear demonstration of the results, the frequency $\omega(k_1, k_2)$ is normalized with respect to ω_0 as $\Omega = \omega/\omega_0$, where $\omega_0 = \frac{\pi^2}{L^2}\sqrt{\frac{EI}{\rho A}}$ is the first flexural frequency of the simply-supported Euler-Bernoulli beam of the length L. The number of finite elements per beam in the unit cell is adopted as $n_{ele} = 25$.

It is practical to assume that all realizations corresponding to these random parameters will be positive and therefore, they are assumed to be log-normally distributed. However, the ML-based stochastic wave propagation framework employed here is generalized so that it can deal with all possible probabilistic distributions. The description of the random parameters is provided in Table 1. The wave response of the lattice structure in the form of the dispersion curve is the

Table 1: Description of random parameters considered for the stochastic wave propagation analysis

Variables	Distribution	Mean	C.O.V.
Elastic modulus E	Lognormal	2.1×10^{11}	0.05
Density ρ	Lognormal	25×10^3	0.05
Poisson's ratio ν	Lognormal	0.25	0.05
Wall slenderness ratio β	Lognormal	1/15	0.05

stochastic output quantity of interest. Four ML techniques, namely Gaussian process, artificial

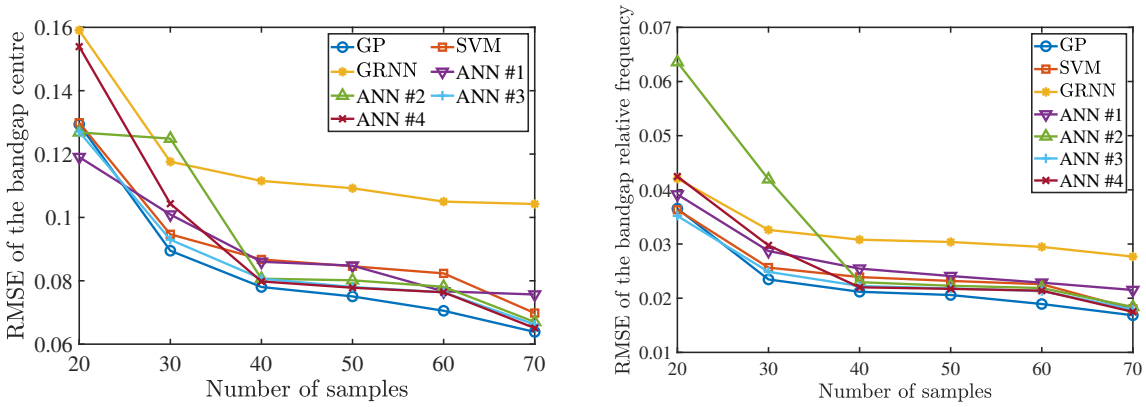

(a) RMSE of the bandgap centre

(b) RMSE of the bandgap relative frequency

Figure 5: Convergence of the root mean squared error of the bandgap (a) centre and (b) relative frequency for selecting the number of samples to build the machine learning models.

neural network, radial basis neural network and support vector machine, have been studied to approximate the overall stochastic wave response by using a nominal number of high-fidelity computations. For training all the ML models, the Latin hypercube sampling (LHS) scheme [66] is used. This was implemented with the help of the "lhsdesign" built-in function of MATLAB and the "maximin" option which maximises the minimum distance between points.

Convergence of the root mean squared error (RMSE) in approximating the bandgap has been carried out to select the number of training points for building the models as presented in Fig. 5. Since the variation in the bandgap can significantly affect the application of periodic lattice systems as wave filters in vibration isolation applications, it is explicitly studied. For quantifying the variation in the bandgap, the centre position and relative frequency (a measure of the width) of the bandgap is determined by Eqs. (23) and (24), respectively.

$$\text{Bandgap centre} = (\omega_u + \omega_l)/2 \tag{23}$$

$$\text{Relative frequency of bandgap} = (\omega_u - \omega_l)/(\omega_u + \omega_l)/2 \tag{24}$$

where, ω_u and ω_l represent the upper and lower frequency boundary of the band gap, respectively. From Fig. 5, the number of training points is selected to be 50. For a fair comparison of the ML techniques, the training data set is equal size and consists of the same sample points. Note that after building the ML models using these 50 samples, the RMSE reported in Fig. 5 has been calculated with respect to 5000 samples of MCS (test data set). Therefore, the ML models are validated on an unknown (test) dataset and the error reported represents test RMSE. For an unbiased assessment of the ML techniques, they are tested on the same test data set.

The DACE platform was employed to implement the GP model in this work [57]. A Gaussian correlation function was assumed to construct the GP. It can be observed from Fig. 5, that four MLP models were utilized for the convergence study. ANN #1, ANN #2, ANN #3 and ANN #4 represent artificial neural networks with 1 layer (10 neurons), 1 layer (50 neurons), 2 layers (10 neurons per layer), and 2 layers (20 neurons each layer), respectively. Out of these four ANN models, ANN #3 (the model with 2 layers and 10 neurons per layer) is selected based on the stable convergence and slight difference compared to ANN #4 (ANN #4 being slightly more accurate for samples over 40, as expected due to the denser configuration). So, from now onwards, the selected ANN #3 model will be referred to as ANN or MLP for the subsequent analysis. The back-propagation algorithm utilizes Levenberg-Marquardt optimization. The radial basis neural network (RBNN) used here has a radial basis layer and a special linear layer. The first layer

operates just like the radial basis layer and has as many neurons as there are input/ target vectors. Each neuron's weighted input is the distance between the input vector and its weight vector. Each neuron's net input is the product of its weighted input with its bias. The implementation details of RBNN can be found in the 'GRNN' page of MATLAB help documentation. The SVM model utilizes a Gaussian kernel and the operations are computed on the standardized data. Note that in constructing the neural network (NN) models, MLP and RBNN, their multi-output configuration is used. This means that each frequency corresponding to the entire range of wave vector is approximated by a single NN model. Thus, if one investigates the first 15 natural frequencies of the lattice system, 15 NN models are required. Whereas GP and SVM are used in their single-output configuration, which means one separate model is required to approximate a frequency value (scalar) corresponding to each wave vector value.

The band plots of dispersion curves are presented in Fig. 6. It is evident from the wide bands of frequencies that micro-structural uncertainty can lead to significant variation in the wave response of lattice structures. The effect of input (material and geometric) variability has been shown to be inconsequential in the low-frequency regime in Fig. 6. The reason is that the associated wavelength of those frequencies is much larger than the size of the unit-cell. This observation is in line with the existing literature. It was further observed that the wall slenderness ratio β representative of the lattice geometry in this study is found to be significantly more sensitive compared to the material properties. However, quantitative assessment of the individual sensitivity will require further investigation as the response quantities are multi-output in nature due to the modes varying in the k-space and thus, is expected to be more computationally expensive than conventional stochastic sensitivity analysis. It can be observed that striking similarity has been achieved between the ML (approximate) and MCS (actual) based stochastic wave response. From these results, it is reasonable to infer that the ML techniques have performed satisfactorily in capturing the response trends in nominal computational cost.

Note that the bandgap has been indicated by a light yellow band in Fig. 6. The variation in the bandgap centre position and relative frequency of the bandgap have been studied in Figs. 7 and 9, respectively. Since the difference of the variation of bandgap centres is not clear from Fig. 7, the probability density functions (PDF) of the bandgap centres at the four points of IRBZ (refer Fig. 2) obtained by the ML techniques are presented in Fig. 8. It can be observed from the results that all the ML techniques have performed well in capturing the overall variation in the centre position and relative frequency of the bandgap. Only the approximation of bandgap centre by RBNN in Fig. 7d is relatively poor (also evident from Fig. 8d). Although the mean of the bandgap centre is well estimated, the extremum points are slightly overestimated. This can be improved either by tuning some of the network parameters or increasing the number of training samples. Having said this, the performance of RBNN is not even close to being unacceptable considering significantly fewer models are employed for RBNN compared to GP and SVM. Note that instead of the above ML techniques, any other approaches can be easily fused in the above non-intrusive stochastic framework, provided it is capable of capturing the highly sensitive non-linear wave response variation.

4.2. Analysis at the global structural level

To verify the results of the above frequency band structures obtained by considering the Bloch theorem and unit cell, frequency response functions (FRF) corresponding to a rectangular plate-like structure for clamped-free-free-free (CFFF) boundary conditions, as shown in Fig. 10, have been determined.

The stochastic dynamic response of the structural system considered in Fig. 10 has been investigated. The length and width of the finite dimension honeycomb lattice structure are related

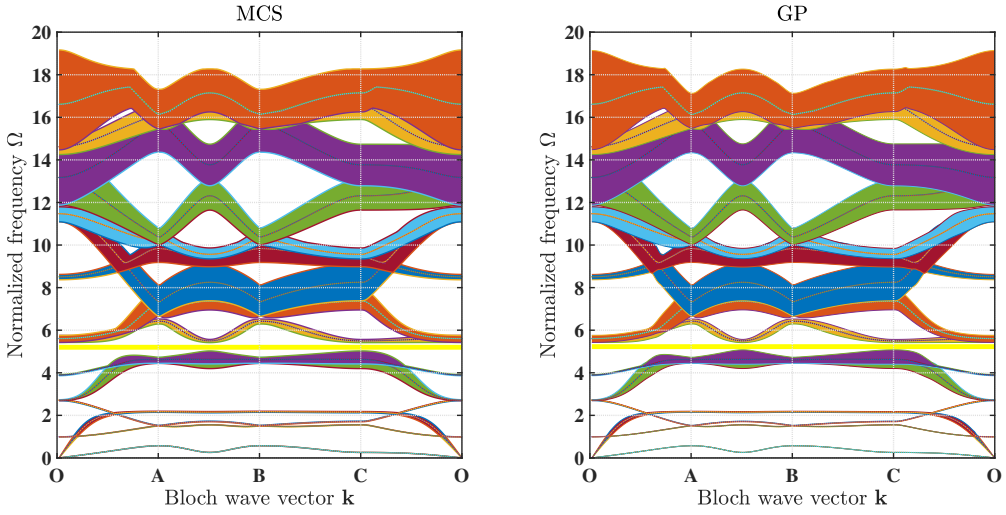

(a) MCS

(b) Gaussian process (GP)

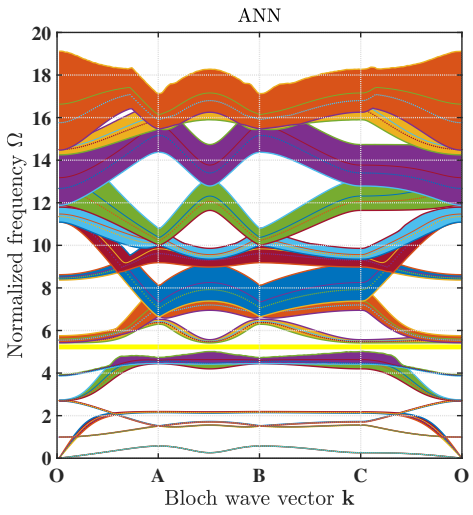

(c) Multi-layer perceptron (MLP

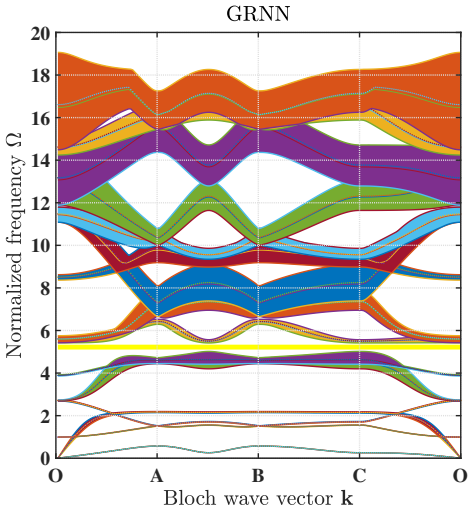

(d) Radial basis neural network (RBNN)

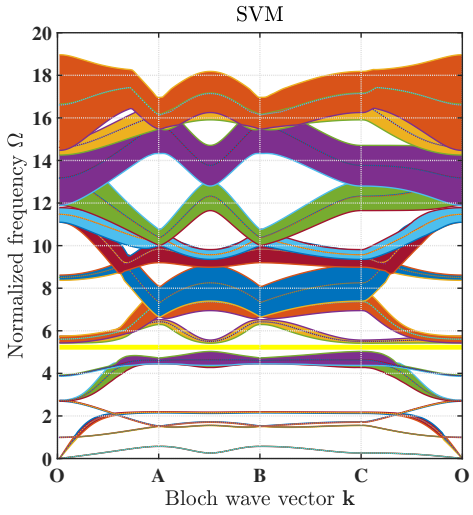

(e) Support vector machine (SVM)

Figure 6: Stochastic dispersion curves with the bandgap highlighted in yellow colour (between ordinate value 4 and 6) by (a) Monte Carlo simulation (5000 samples) (b) Gaussian process (c) Multi-layer perceptron (d) Radial basis neural network (e) Support vector machine. For a fair comparison, models (b)-(e) are trained using the same set of 50 samples. In the y-axis, the frequency $\omega(k_1, k_2)$ is normalized with respect to ω_0 as $\Omega = \omega/\omega_0$, where $\omega_0 = \frac{\pi^2}{L^2}\sqrt{\frac{EI}{\rho A}}$ is the first flexural frequency of the simply-supported Euler-Bernoulli beam of the length L. The x-axis represents the k-space within the FBZ as shown in Fig. 2. 200 k values are considered to simulate the FBZ with 50 values for each of the four boundary divisions ($O - A - B - C - O$).

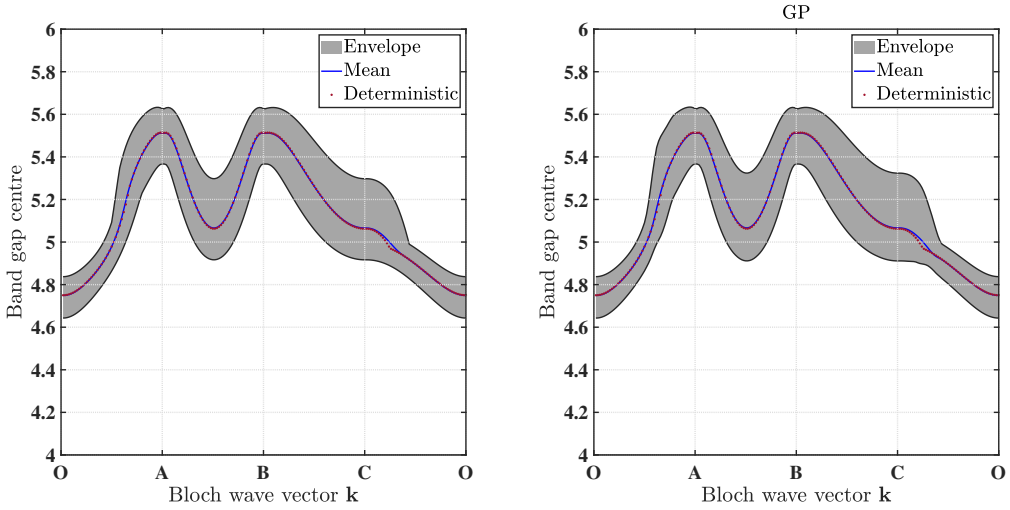

(a) MCS

(b) Gaussian process (GP)

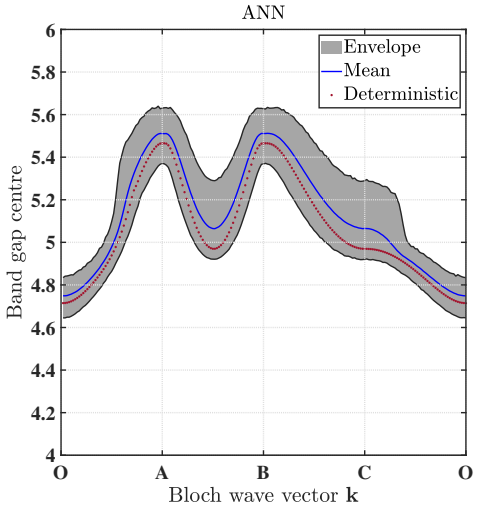

(c) Multi-layer perceptron (MLP)

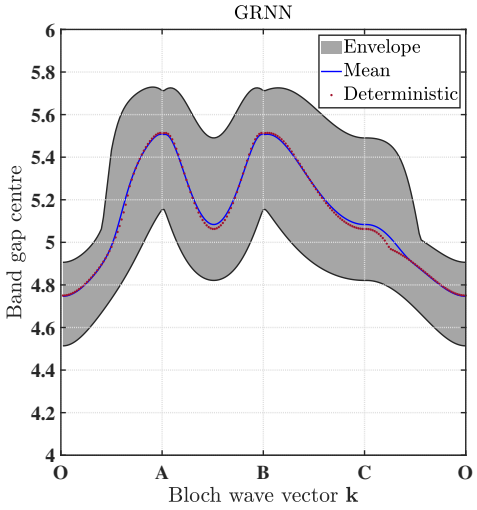

(d) Radial basis neural network (RBNN)

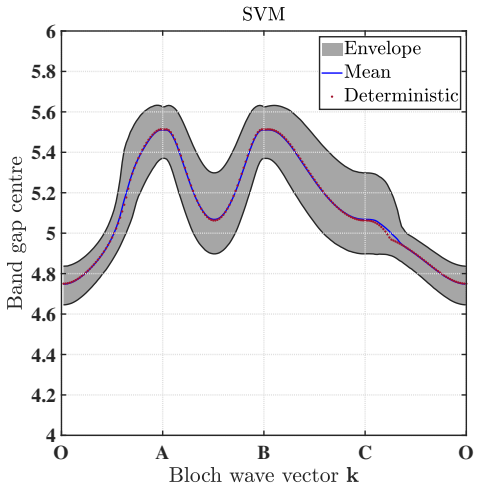

(e) Support vector machine (SVM)

Figure 7: Variation of the bandgap centre by (a) Monte Carlo simulation (5000 samples) (b) Gaussian process (c) Multi-layer perceptron (d) Radial basis neural network (e) Support vector machine. For a fair comparison, models (b)-(e) are trained using the same set of 50 samples. The deterministic bandgap centre (in red dots) was evaluated at the nominal (mean) values of the random input parameters. The mean bandgap centre (in blue) is the average of the envelope corresponding to the random realizations for each wave vector value. The bandgap centre represented on the y-axis has been computed using Eq. (23). The x-axis represents the k-space within the FBZ as shown in Fig. 2. 200 k values are considered to simulate the FBZ with 50 values for each of the four boundary divisions ($O - A - B - C - O$).

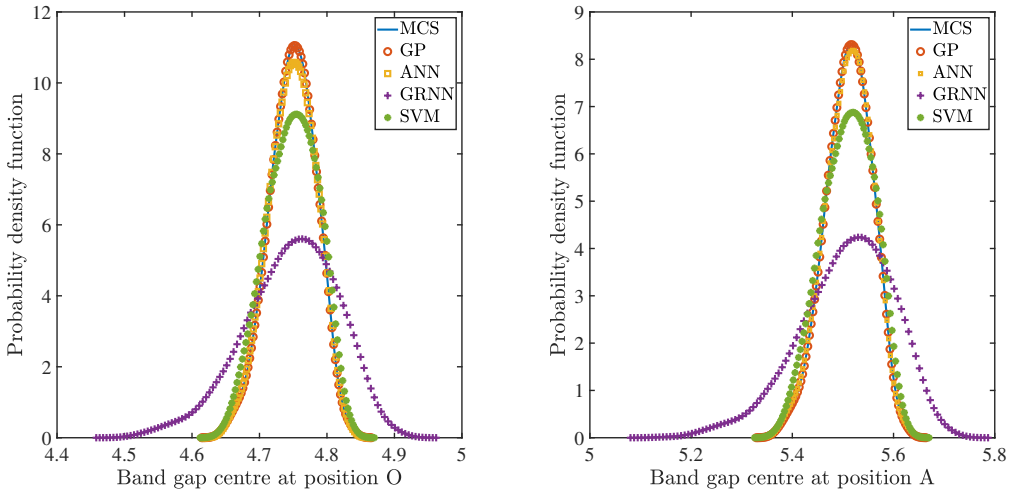

(a) PDF of bandgap centre at O

(b) PDF of bandgap centre at A

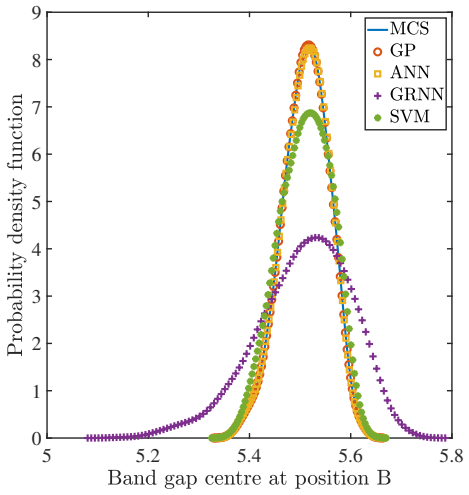

(c) PDF of bandgap centre at B

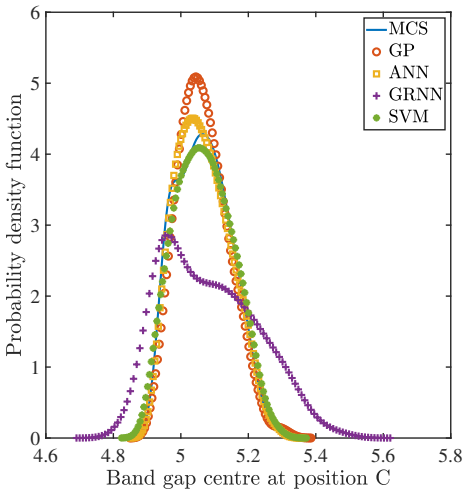

(d) PDF of bandgap centre at C

Figure 8: Probability density functions at various positions of irreducible Brillouin zone (a) O (b) A (c) B (d) C.

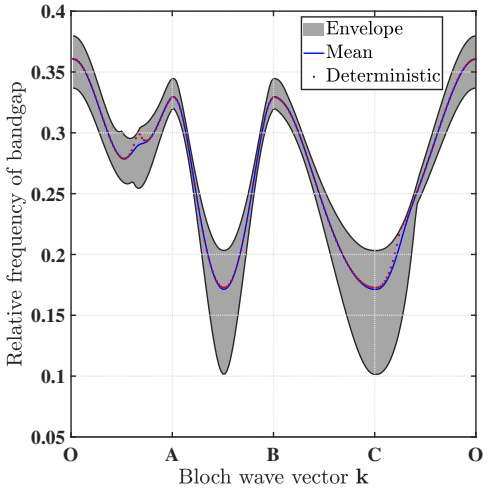

(a) MCS

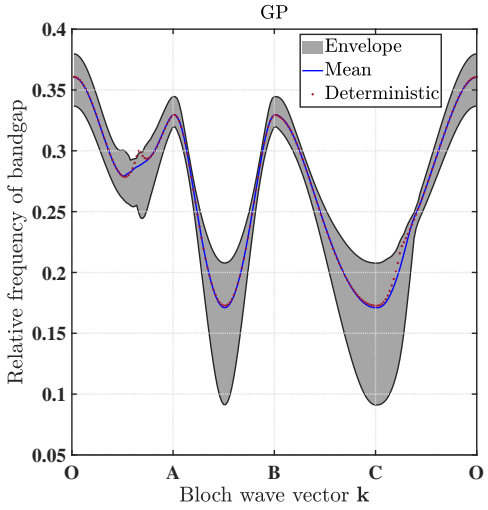

(b) Gaussian process (GP)

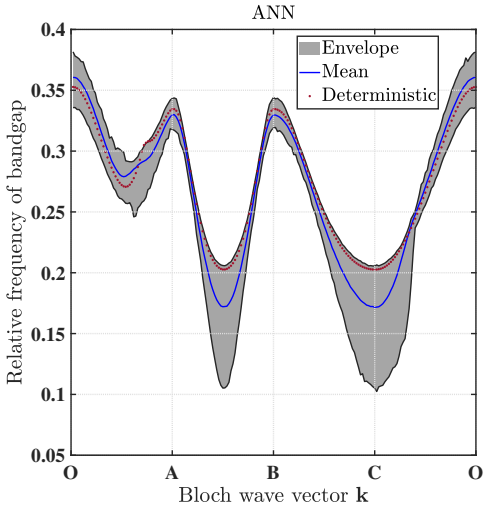

(c) Multi-layer perceptron (MLP)

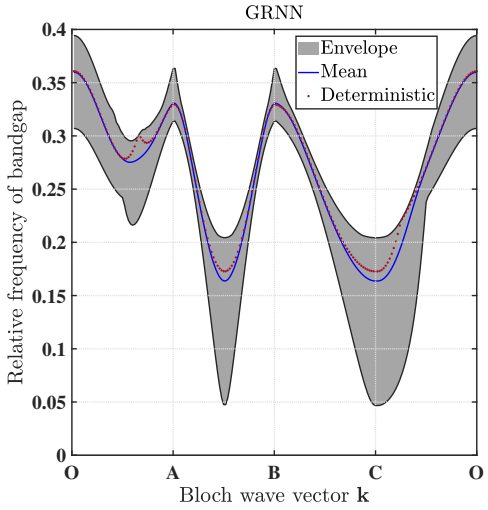

(d) Radial basis neural network (RBNN)

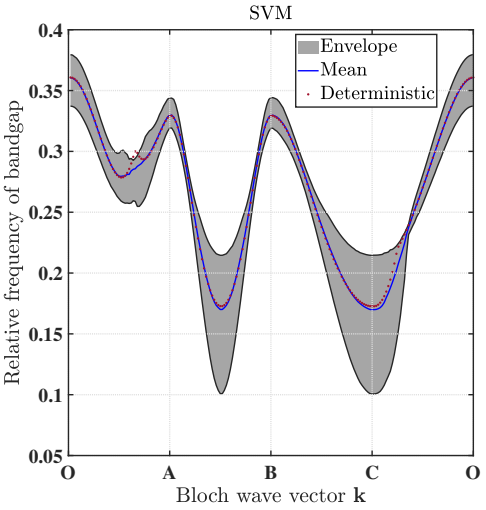

(e) Support vector machine (SVM)

Figure 9: Variation of the relative frequency of bandgap by (a) Monte Carlo simulation (5000 samples) (b) Gaussian process (c) Multi-layer perceptron (d) Radial basis neural network (e) Support vector machine. For a fair comparison, models (b)-(e) are trained using the same set of 50 samples. The deterministic relative frequency of bandgap (in red dots) was evaluated at the nominal (mean) values of the random input parameters. The mean relative frequency (in blue) is the average of the envelope corresponding to the random realizations for each wave vector value. The bandgap relative frequency represented on the y-axis has been computed using Eq. (24). The x-axis represents the k-space within the FBZ as shown in Fig. 2. 200 k values are considered to simulate the FBZ with 50 values for each of the four boundary divisions ($O - A - B - C - O$).

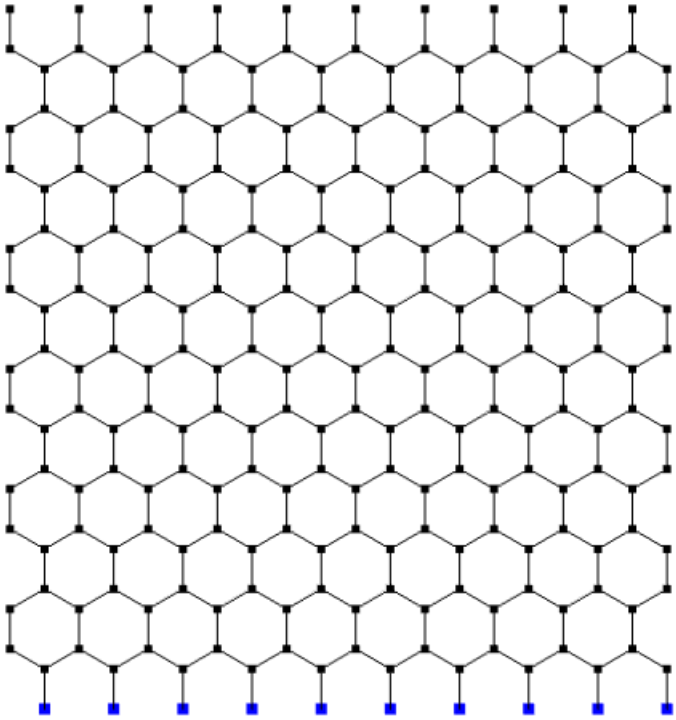

Figure 10: The finite dimensional lattice honeycomb structure with clamped-free-free-free boundary conditions. The blue color marked points represent the fixed points of clamped boundary condition.

to the length of the beam segment L and lattice angle θ. The input uncertainty has been assumed at the unit cell level and is same as that of the stochastic wave propagation analysis performed above (refer Table 1). This analysis is intended towards quantifying the effect of micro-structural anomalies on the global dynamic behaviour of the structural system. The input uncertainty in the form of material and geometric parameters at the unit cell level of the lattice system is propagated to the global mass and stiffness matrices, and a stochastic eigenvalue problem is posed taking into account the global random system matrices (comprising 3420 DOFs) for the undamped case. Corresponding to a random realization of the modal solutions, FRFs are obtained. For validation of the location of the bandgap at the unit cell and global structural level, the undamped deterministic dispersion curve and deterministic FRF with negligible damping (0.01 %) have been compared in Figs. 11a and 11b, respectively. The band plot of FRF considering random input parameters has been presented in Fig. 11c. Figure 11 illustrates that the position of the bandgap at the unit cell and global structural level is the same, which validates the model.

Next, the performance of the ML techniques has been assessed in the context of their approximation capability of the frequency response at the global structural level. For this, each of the modal solutions is represented by individual ML techniques. Corresponding to a random realization of the modal solutions, FRFs are obtained considering 0.5% damping. Consequently, the propagation of the input uncertainty to the dynamic response using the ML techniques only require a nominal number of analytical or FE simulations of the actual system. The computational efficiency achieved by ML has been quantified later. For training the ML models, the same set of 50 training samples are employed as selected previously from the convergence study in Fig. 5. The configuration of the ML models is also the same as above. For validation, 1000 samples of MCS (test data set) are used. The variation of the FRFs are presented in Figs. 12 and 13.

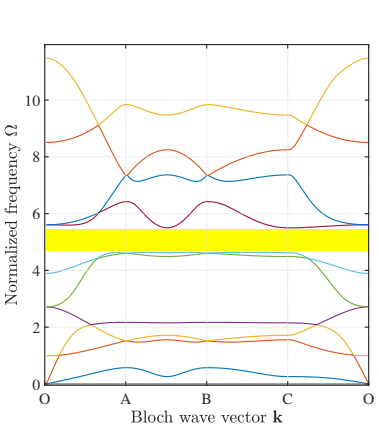

(a) Deterministic dispersion curve

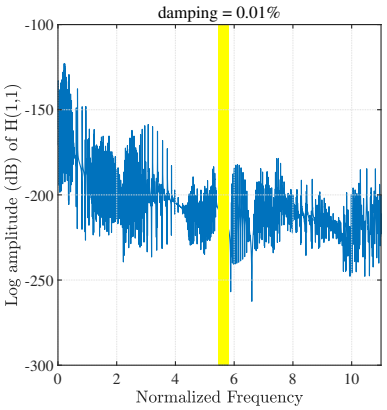

(b) Deterministic FRF H(1,1)

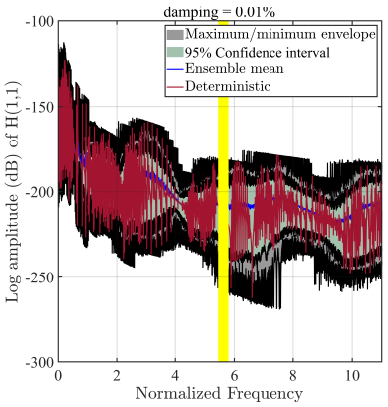

(c) Stochastic FRF H(1,1) obtained by MCS

Figure 11: Validation of the bandgap at the (a) unit cell level (deterministic) (b) global structural level (deterministic) (c) global structural level (stochastic). Frequency response functions in (b) and (c) are obtained corresponding to 0.01% damping. (c) is obtained by 1000 Monte Carlo simulations.

Sample direct and cross FRF band plots corresponding to the DOFs of edge nodes are presented in Figs. 12 and 13, respectively. Specifically nodes at the edges have been selected for demonstration as it would be convenient to experimentally measure the FRFs at these locations from a practical point of view. Note that the bandgaps are not identifiable from the sample FRF plots in Figs. 12 and 13 as the bandgaps are essentially obtained from undamped eigenvalue analysis whereas the FRFs are evaluated considering 0.5 % damping. The higher damping (compared to 0.01 % damping in Fig. 11c) averages out the frequency response as evident from the ensemble mean FRFs which makes the bandgap disappear. In general, it can be observed from Figs. 12 and 13 that close proximity has been achieved between the ML (approximate) and MCS (actual) based stochastic frequency response. It can be visually observed that the performance of RBNN in capturing the overall response variation is not as robust as the other ML techniques used. This can possibly be improved either by tuning some of the network parameters or increasing the number of training samples. For an explicit assessment of the approximation accuracy achieved by the ML models, the RMSE of the mean and standard deviation of the FRFs are presented in Table 2.

Table 2: Root mean squared error of the mean and standard deviation of the frequency response functions obtained by the machine learning models. Note that the errors of the response statistics have been computed with respect to Monte Carlo simulations. SD denotes standard deviation.

Response quantities	GP	ANN	GRNN	SVM
mean H(1,1) $\times 10^{-9}$	0.2175	1.1682	2.0582	1.9843
SD H(1,1) $\times 10^{-8}$	0.0319	0.1525	1.0373	1.0253
mean H(1,1132) $\times 10^{-9}$	0.3350	1.8021	3.2730	3.0245
SD H(1,1132) $\times 10^{-8}$	0.0513	0.2252	1.5784	1.5308
mean H(1132,1132) $\times 10^{-9}$	0.5270	4.4150	9.8837	9.3358
SD H(1132,1132) $\times 10^{-8}$	0.1107	0.5370	4.3010	4.2057

To analyze the global structure comprising 3420 DOFs, significant computational savings was achieved by the ML models, which is quantified next. The time required to perform a single eigenvalue analysis took around 480 s on an Intel® Xeon® W-2145 CPU @ 3.70 GHz, 3696 MHz, with 8 cores and 16 logical processors. Hence, the time required for 1000 MCS samples was (1000

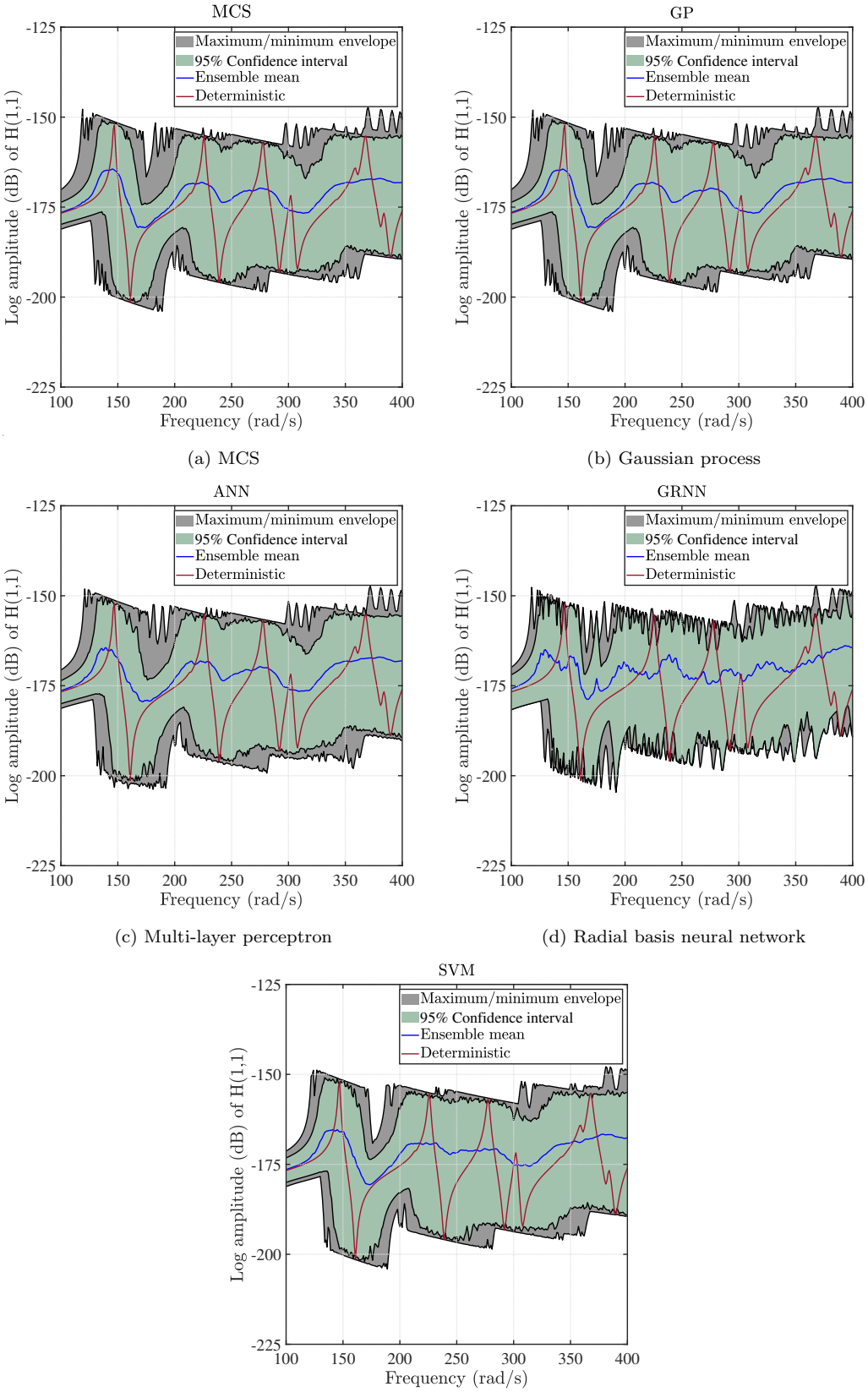

(a) MCS

(b) Gaussian process

(c) Multi-layer perceptron

(d) Radial basis neural network

(e) Support vector machine

Figure 12: Sample direct frequency response function H(1,1) band plots (a) Monte Carlo simulation (1000 samples) (b) Gaussian process (c) Multi-layer perceptron (d) Radial basis neural network (e) Support vector machine. For a fair comparison, models (b)-(e) are trained using the same set of 50 samples. The grey envelope represents the maximum/minimum points. The green envelope represents the 95% confidence interval points. The deterministic frequency response function (in red) was evaluated at the nominal (mean) values of the random input parameters. The ensemble mean frequency response function (in blue) is the average of the envelope corresponding to the random realizations for each forcing frequency value.

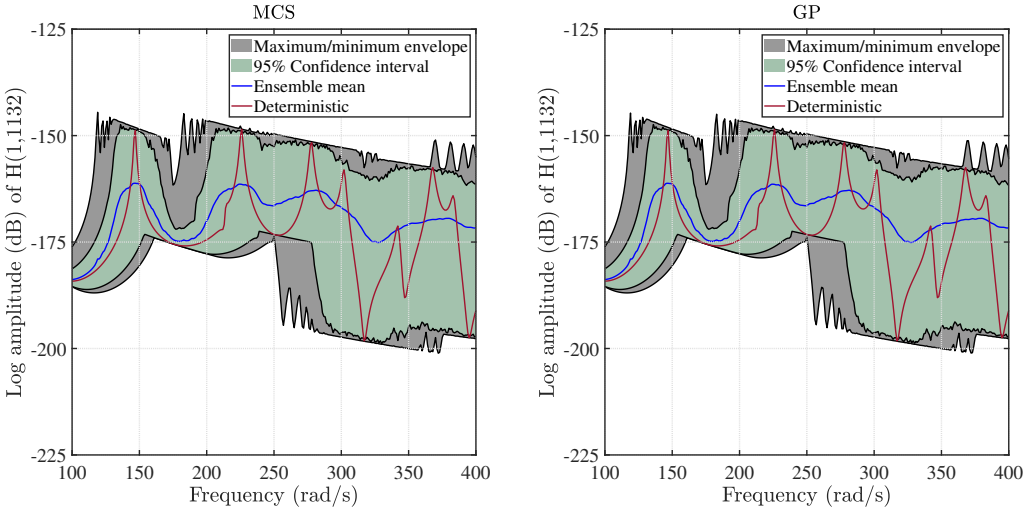

(a) MCS

(b) Gaussian process

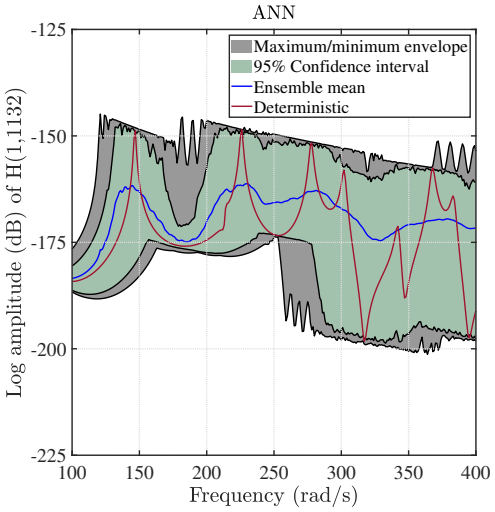

(c) Multi-layer perceptron

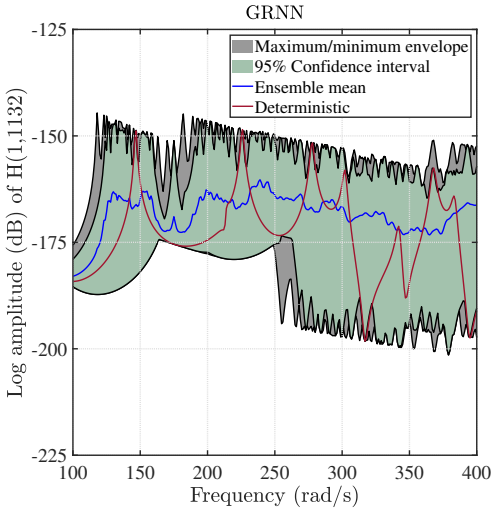

(d) Radial basis neural network

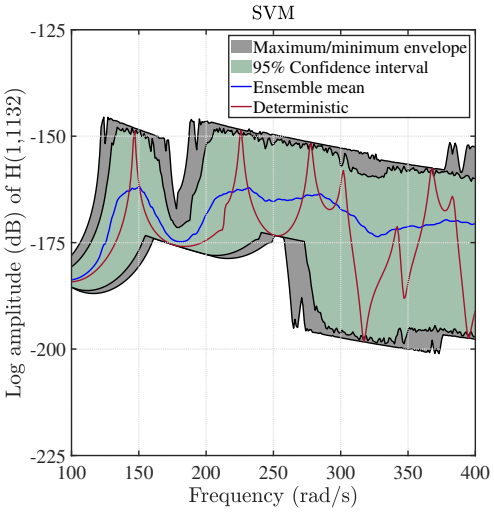

(e) Support vector machine

Figure 13: Sample cross frequency response function H(1,1132) band plots (a) Monte Carlo simulation (1000 samples) (b) Gaussian process (c) Multi-layer perceptron (d) Radial basis neural network (e) Support vector machine. For a fair comparison, models (b)-(e) are trained using the same set of 50 samples. The grey envelope represents the maximum/minimum points. The green envelope represents the 95% confidence interval points. The deterministic frequency response function (in red) was evaluated at the nominal (mean) values of the random input parameters. The ensemble mean frequency response function (in blue) is the average of the envelope corresponding to the random realizations for each forcing frequency value.

$\times$ 480) s, equivalent to 5.56 days. The time required to generate samples for the ML models was (50 $\times$ 480) s, equivalent to 6.67 hours. The model building time required by GP, ANN, RBNN and SVM was calculated to be 4.34 s, 401.38 s, 61.81 s and 18.39 s, respectively. Consequently, the ML models required 5-5.1 % CPU time compared to MCS for solving the stochastic problem. Thus, from these results, it is reasonable to infer that the ML techniques have performed decently in capturing the response trends with nominal computational cost.

5. Summary and Conclusions

A generalized uncertainty quantification framework for wave propagation and dynamic response analysis of hexagonal lattice structures is presented. The micro-structural variability has been simulated by random material and geometrical properties in the unit cell, retaining the periodicity. Four machine learning techniques, namely, Gaussian process, multi-layer perceptron, radial basis neural network and support vector machine are employed as physics-based metamodels to mimic the stochastic wave response of the periodic lattice system with significantly reduced computational effort. To the advantage of the interested reader, user-friendly toolboxes of these four ML techniques are available in MATLAB. Based on the results obtained, the key take-aways from the study include:

1. Input uncertainties result in wide variation in the wave response, bandgap and global dynamic behaviour. This reveals that uncertainty associated with periodic structures should be considered in (highly sensitive) mechanical applications of periodic structures for e.g., wave filter design for vibration mitigation.
2. All the machine learning techniques perform satisfactorily in capturing the stochastic wave and dynamic response of lattice structure.
3. The machine learning techniques implemented in multi-output configurations, namely multi-layer perceptron and radial basis neural network, are observed to achieve a similar level of accuracy in spite of using fewer models compared to the approaches employed in single-output configurations (Gaussian process and support vector machine).
4. The proposed stochastic framework is completely generalized and non-intrusive so that it can handle the following,
   (a) different probabilistic variation of the input random parameters,
   (b) quantify uncertainties in the parametric space both at an individual or combined level,
   (c) analyze other lattice geometries as long as their periodicity is retained,
   (d) integrate other sampling schemes,
   (e) integrate other ML techniques or surrogate models provided they are capable of capturing the nonlinear response trends, and
   (f) the in-house code implementation allows automated detection of bandgaps without manual intervention.
5. The savings in the computational cost by employing machine learning techniques have been better realized when the analysis was up-scaled from the unit cell level to the macro-scale continuum structural level.

Limitations of the work include, parametric uncertainty models were considered here, which do not account for the spatial variability in the micro-structure. Also, the model assumes perfect periodicity and does not consider local defects or damage within the unit cell. These can be potential future works. Another interesting future application of the ML-based proposed framework will be for computationally expensive reliability-based and/or robust design optimization of lattice periodic structures, where UQ is coupled within the optimization loop and

involves a significantly high number of high-fidelity simulations. The proposed meta-modelling scheme can prove to be much effective to reduce the computational cost. The variation in the wave and dynamic response behaviour offer a feasible solution to define manufacturing tolerances for hexagonal periodic structures in order to obtain a bandgap behaviour within certain requirements. This is critical for the technology transfer of the promising results presented in scientific studies into industrial applications not limited to robust design of filters and insulators for vibration isolation and energy harvesting.

Acknowledgements

Dr. D. Karličić and Prof. S. Adhikari were supported by the Marie Skłodowska-Curie Actions - European Commission: 799201-METACTIVE. Dr. T. Chatterjee and Prof. Michael I. Friswell gratefully acknowledge the support of the Engineering and Physical Sciences Research Council through the award of a Programme Grant "Digital Twins for Improved Dynamic Design", grant number EP/R006768.

Data Availability Statement

The raw/processed data required to reproduce these findings cannot be shared at this time as the data also forms part of an ongoing study.

References

[1] L. Solymar, E. Shamonina, Waves in Metamaterials, Oxford University Press, Inc., USA, 2009.
[2] J. Christensen, M. Kadic, O. Kraft, M. Wegener, Vibrant times for mechanical metamaterials, Mrs Communications 5 (3) (2015) 453–462.
[3] O. Sigmund, J. Jensen, Systematic design of phononic band-gap materials and structures by topology optimization, Philosophical Transactions of the Royal Society London, Series A (Mathematical, Physical and Engineering Sciences) 361 (2003) 1001–1019.
[4] J. U. Surjadi, L. Gao, H. Du, X. Li, X. Xiong, N. X. Fang, Y. Lu, Mechanical metamaterials and their engineering applications, Advanced Engineering Materials 21 (3) (2019) 1800864.
[5] S. Gonella, M. Ruzzene, Analysis of in-plane wave propagation in hexagonal and re-entrant lattices, Journal of Sound and Vibration 312 (1-2) (2008) 125–139.
[6] K. Zhang, Y.-c. Su, X.-h. Hou, J.-m. Meng, Z.-c. Deng, Effect of pre-load on wave propagation characteristics of hexagonal lattices, Composite Structures 203 (2018) 361–372.
[7] M. S. Mazloomi, M. Ranjbar, L. Boldrin, F. Scarpa, S. Patsias, N. Ozada, Vibroacoustics of 2d gradient auxetic hexagonal honeycomb sandwich panels, Composite Structures 187 (2018) 593–603.
[8] K. Zhang, P. Zhao, C. Zhao, F. Hong, Z. Deng, Study on the mechanism of band gap and directional wave propagation of the auxetic chiral lattices, Composite Structures 238 (2020) 111952.
[9] D. Karličić, M. Cajić, T. Chatterjee, S. Adhikari, Wave propagation in mass embedded and pre-stressed hexagonal lattices, Composite Structures 256 (2021) 113087.
[10] Y. Iwata, T. Yokozeki, Shock wave filtering of two-dimensional cfrp x-lattice structures: A numerical investigation, Composite Structures 265 (2021) 113743.
[11] Y. Iwata, T. Yokozeki, Wave propagation analysis of one-dimensional cfrp lattice structure, Composite Structures 261 (2021) 113306.
[12] X. Xiao, Z. He, E. Li, B. Zhou, X. Li, A lightweight adaptive hybrid laminate metamaterial with higher design freedom for wave attenuation, Composite Structures 243 (2020) 112230.
[13] J. Li, P. Yang, S. Li, Phononic band gaps by inertial amplification mechanisms in periodic composite sandwich beam with lattice truss cores, Composite Structures 231 (2020) 111458.
[14] V. E. Gasparetto, M. S. ElSayed, Multiscale optimization of specific elastic properties and microscopic frequency band-gaps of architectured microtruss lattice materials, International Journal of Mechanical Sciences 197 (2021) 106320.

[15] M. Ayad, N. Karathanasopoulos, H. Reda, J. Ganghoffer, H. Lakiss, Dispersion characteristics of periodic structural systems using higher order beam element dynamics, Mathematics and Mechanics of Solids 25 (2) (2020) 457–474.
[16] H. Reda, N. Karathanasopoulos, J. Ganghoffer, H. Lakiss, Wave propagation characteristics of periodic structures accounting for the effect of their higher order inner material kinematics, Journal of Sound and Vibration 431 (2018) 265–275.
[17] H. Reda, Y. Rahali, J. Ganghoffer, H. Lakiss, Wave propagation analysis in 2d nonlinear hexagonal periodic networks based on second order gradient nonlinear constitutive models, International Journal of Non-Linear Mechanics 87 (2016) 85–96.
[18] N. Karathanasopoulos, H. Reda, J. Ganghoffer, The role of non-slender inner structural designs on the linear and non-linear wave propagation attributes of periodic, two-dimensional architectured materials, Journal of Sound and Vibration 455 (2019) 312–323.
[19] R. K. Pal, M. Ruzzene, J. J. Rimoli, Tunable wave propagation by varying prestrain in tensegrity-based periodic media, Extreme Mechanics Letters 22 (2018) 149–156.
[20] K. Pajunen, P. Celli, C. Daraio, Prestrain-induced bandgap tuning in 3d-printed tensegrity-inspired lattice structures, Extreme Mechanics Letters 44 (2021) 101236.
[21] K. Liu, T. Zegard, P. P. Pratapa, G. H. Paulino, Unraveling tensegrity tessellations for metamaterials with tunable stiffness and bandgaps, Journal of the Mechanics and Physics of Solids 131 (2019) 147–166.
[22] P. Celli, S. Gonella, V. Tajeddini, A. Muliana, S. Ahmed, Z. Ounaies, Wave control through soft microstructural curling: bandgap shifting, reconfigurable anisotropy and switchable chirality, Smart Materials and Structures 26 (3) (2017) 035001.
[23] C. Nimmagadda, K. H. Matlack, Thermally tunable band gaps in architected metamaterial structures, Journal of Sound and Vibration 439 (2019) 29–42.
[24] Y. Wu, X. Y. Lin, H. X. Jiang, A. G. Cheng, Finite element analysis of the uncertainty of physical response of acoustic metamaterials with interval parameters, International Journal of Computational Methods 17 (08) (2020) 1950052.
[25] M. Schevenels, B. Lazarov, O. Sigmund, Robust topology optimization accounting for spatially varying manufacturing errors, Computer Methods in Applied Mechanics and Engineering 200 (49) (2011) 3613–3627.
[26] P. Celli, B. Yousefzadeh, C. Daraio, S. Gonella, Bandgap widening by disorder in rainbow metamaterials, Applied Physics Letters 114 (2019) 091903.
[27] J. Henneberg, J. S. Gomez Nieto, K. Sepahvand, A. Gerlach, H. Cebulla, S. Marburg, Periodically arranged acoustic metamaterial in industrial applications: The need for uncertainty quantification, Applied Acoustics 157 (2020) 107026.
[28] P.-R. Wagner, V. K. Dertimanis, E. N. Chatzi, J. L. Beck, Robust-to-uncertainties optimal design of seismic metamaterials, Journal of Engineering Mechanics 144 (3) (2018) 04017181.
[29] K.-C. Chuang, Z.-Q. Zhang, H.-X. Wang, Experimental study on slow flexural waves around the defect modes in a phononic crystal beam using fiber bragg gratings, Physics Letters A 380 (47) (2016) 3963 – 3969.
[30] Z.-J. Yao, G.-L. Yu, Y.-S. Wang, Z.-F. Shi, Propagation of bending waves in phononic crystal thin plates with a point defect, International Journal of Solids and Structures 46 (13) (2009) 2571 – 2576.
[31] J.-M. Mencik, D. Duhamel, A wave finite element-based approach for the modeling of periodic structures with local perturbations, Finite Elements in Analysis and Design 121 (2016) 40 – 51.
[32] X. N. Do, H. Reda, J. F. Ganghoffer, Impact of damage on the effective properties of network materials and on bulk and surface wave propagation characteristics, Continuum Mechanics and Thermodynamics 33 (2) (2021) 369–401.
[33] H. Reda, Y. Rahali, B. Vieille, H. Lakiss, J. Ganghoffer, Impact of damage on the propagation of rayleigh waves in lattice materials, International Journal of Damage Mechanics 30 (5) (2021) 665–680.
[34] S. Dey, T. Mukhopadhyay, S. Adhikari, Uncertainty Quantification in Laminated Composites: A Meta-model Based Approach, Taylor & Francis Inc (CRC Press), Boca Raton, FL, USA, 2018.
[35] H. A. Babaa, S. Nandi, T. Singh, M. Nouh, Uncertainty Quantification of Tunable Elastic Metamaterials using Polynomial Chaos, Journal of Applied Physics 127 (2020) 015102.
[36] T. Chatterjee, D. Karličić, S. Adhikari, M. I. Friswell, Gaussian process assisted stochastic dynamic analysis with applications to near-periodic structures, Mechanical Systems and Signal Processing 149 (2021) 107218.
[37] Z. C. He, J. Y. Hu, E. Li, An uncertainty model of acoustic metamaterials with random parameters, Computational Mechanics 62 (2018) 1023–1036.
[38] D. Beli, A. Fabro, M. Ruzzene, J. R. F. Arruda, Wave attenuation and trapping in 3d printed cantilever-in-mass metamaterials with spatially correlated variability, Scientific Reports 9 (2019) 5617.
[39] A. T. Fabro, H. Meng, D. Chronopoulos, Uncertainties in the attenuation performance of a multi-frequency

metastructure from additive manufacturing, Mechanical Systems and Signal Processing 138 (2020) 106557.
[40] D. Finol, Y. Lu, V. Mahadevan, A. Srivastava, Deep convolutional neural networks for eigenvalue problems in mechanics, International Journal for Numerical Methods in Engineering 118 (5) (2019) 258–275.
[41] A. Bacigalupo, G. Gnecco, M. Lepidi, L. Gambarotta, Machine-learning techniques for the optimal design of acoustic metamaterials, Journal of Optimization Theory and Applications 187 (3) (2020) 630–653.
[42] F. Bloch, Quantum mechanics of electrons in crystal lattices, Z. Phys 52 (1928) 555–600.
[43] M. I. Hussein, M. J. Leamy, M. Ruzzene, Dynamics of phononic materials and structures: Historical origins, recent progress, and future outlook, Applied Mechanics Reviews 66 (4) (2014) 040802.
[44] M. Collet, M. Ouisse, M. Ruzzene, M. Ichchou, Floquet–bloch decomposition for the computation of dispersion of two-dimensional periodic, damped mechanical systems, International Journal of Solids and Structures 48 (20) (2011) 2837–2848.
[45] M. J. Leamy, Exact wave-based bloch analysis procedure for investigating wave propagation in two-dimensional periodic lattices, Journal of Sound and Vibration 331 (7) (2012) 1580–1596.
[46] C. Kittel, P. McEuen, P. McEuen, Introduction to solid state physics, Vol. 8, Wiley New York, 1996.
[47] J. Meng, Z. Deng, K. Zhang, X. Xu, Wave propagation in hexagonal and re-entrant lattice structures with cell walls of non-uniform thickness, Waves in Random and Complex Media 25 (2) (2015) 223–242.
[48] J. V. Scheidt, W. Purkert, Random Eigenvalue Problems, North Holland, New York, 1983.
[49] S. Adhikari, Joint statistics of natural frequencies of stochastic dynamic systems, Computational Mechanics 40 (4) (2007) 739–752.
[50] D. G. Krige, A Statistical approach to some basic mine valuation problems on the witwatersrand, Journal of the Chemical, Metallurgical and Mining Society of South Africa 52 (6) (1951) 119 – 139.
[51] F. A. DiazDelaO, S. Adhikari, Structural dynamic analysis using gaussian process emulators, Engineering Computations 27 (5) (2010) 580–605.
[52] T. Chatterjee, S. Adhikari, M. I. Friswell, Uncertainty propagation in dynamic sub-structuring by model reduction integrated domain decomposition, Computer Methods in Applied Mechanics and Engineering 366 (2020) 113060.
[53] F. A. DiazDelaO, S. Adhikari, Gaussian process emulators for the stochastic finite element method, International Journal of Numerical Methods in Engineering 87 (6) (2011) 521–540.
[54] T. Chatterjee, R. Chowdhury, Adaptive Bilevel Approximation Technique for Multiobjective Evolutionary Optimization, Journal of Computing in Civil Engineering 31 (3) (2017) 04016071.
[55] T. Chatterjee, R. Chowdhury, P. Ramu, Decoupling Uncertainty Quantification from Robust Design Optimization, Structural and Multidisciplinary Optimization 59 (2019) 1969–1990.
[56] C. E. Rasmussen, C. K. I. Williams, Gaussian Processes for Machine Learning, The MIT Press, Cambridge, Massachusetts London, England, 2006.
[57] S. Lophaven, H. Nielson, J. Sondergaard, DACE A MATLAB Kriging Toolbox, Tech. rep., Technical University of Denmark, IMM-TR-2002-12, Technical University of Denmark (2002).
[58] M. Moustapha, J. M. Bourinet, B. Guillaume, B. Sudret, Comparative Study of Kriging and Support Vector Regression for Structural Engineering Applications, Journal of Uncertainty in Engineering Systems, Part A: Civil Engineering 4 (2) (2018) 04018005.
[59] T. Chatterjee, R. Chowdhury, h – p adaptive model based approximation of moment free sensitivity indices, Computer Methods in Applied Mechanics and Engineering 332 (2018) 572–599.
[60] I. Goodfellow, Y. Bengio, A. Courville, Deep learning, MIT press, 2016.
[61] R. Hecht-Nielsen, Applications of counterpropagation networks, Neural networks 1 (2) (1988) 131–139.
[62] D. E. Rumelhart, G. E. Hinton, R. J. Williams, Learning representations by back-propagating errors, Nature 323 (1986) 533–536.
[63] C. Cortes, V. Vapnik, Support-vector networks, Machine learning 20 (3) (1995) 273–297.
[64] B. E. Boser, I. M. Guyon, V. N. Vapnik, A training algorithm for optimal margin classifiers, in: Proceedings of the fifth annual workshop on Computational learning theory, 1992, pp. 144–152.
[65] V. Vapnik, A. Lerner, Generalized portrait method for pattern recognition, Automation and Remote Control 24 (6) (1963) 774–780.
[66] M. McKay, R. J. Beckman, W. J. Conover, A comparison of three methods for selecting values of input variables in the analysis of output from a computer code, Technometrics 21 (2) (1979) 239–245.